Impact of Wastewater Strength and Photocatalyst Loading on Decolourization of Acid Orange 7 by Co-Doped TiO₂

ERICK BUTLER[1,*], OLIVER MULAMBA[1], YUNG-TSE HUNG[2], CHING-CHENG CHEN[3] and YEN-PEI FU[3]

[1]School of Engineering, Computer Science and Mathematics, West Texas A&M University, Canyon, TX 79016, USA
[2]Department of Civil and Environmental Engineering, Cleveland State University, Cleveland, Ohio 44115, USA
[3]Department of Materials Science and Engineering, National Dong Hwa University, Hualien 97401, Taiwan

*Corresponding author: Tel: +1 806 6512271; E-mail: erick.ben.butler@gmail.com

Heterogeneous photocatalysis has proved to be a successful method for the degradation of water pollutants. In this work, the photocatalytic decolourization of acid orange 7 was performed by cobalt-doped titanium dioxide (Co-doped TiO₂). The Co-doped TiO₂ was synthesized and characterized using X-ray diffraction, scanning electron microscopy, energy diffraction spectroscopy, UV-visible reflective dispersion spectroscopy and adsorption of nitrogen gas. The acid orange 7 was prepared as a synthetic textile wastewater at three initial concentrations (24, 34 and 44 mg/L) with three photocatalyst loadings (0.025 g, 0.050, 0.1 g/100 mL acid orange 7). Results show a plateauing behaviour with the effect of photocatalyst concentration on removal of acid orange 7. As the concentration increased of acid orange 7, an ideal photocatalytic loading was found that outperformed higher concentrations in regards to removal of acid orange 7. As such it was concluded that high photocatalyst concentrations are not synonymous with efficient water treatment.

Keywords: Oxides, X-ray photo-emission spectroscopy, Photocatalytic degradation, Optical properties, Wastewater treatment.

INTRODUCTION

There has been a recent interest in using photocatalytic degradation to treat dye wastewater. Photocatalytic degradation of dyes or photocatalysis is an advanced oxidation process (AOP) that typically uses a catalyst (typically a semiconductor) to form the necessary constituents to decolourize a dye species. This affirms the sentiment that the treatment of dye wastewater has evolved from using only conventional sanitary engineering processes to more technologically advanced techniques. Photocatalysis can be used to address the pollutants of concern such as high biological oxygen demand (BOD), chemical oxygen demand (COD) and total suspended solids (TSS), along with toxicity and colour. These pollutants can be created before, during, or after dyeing processes.

There are many other treatment methods available to treat dye wastewater. Some of these methods include aerobic and anaerobic treatment, advanced oxidation processes such as ozone and electrocoagulation. Aerobic and anaerobic treatment are capable of achieving comparable results, but these methods require long retention times [1-3]. Also, some microorganisms that thrive in aerobic environments are incapable of biodegrading because of the xenobiotic constituents present within the wastewater [4,5]. Advanced oxidation processes (AOP) such

as ozone have high energy costs associated with the equipment necessary for ozone generation [6]. Finally, electrochemical methods such as electrocoagulation produce waste from spent electrodes. These electrodes must be either regenerated for reuse or sold as scrap metal. The accumulation of spent electrodes and the process of regenerating or scrapping can make electrocoagulation undesirable. Photocatalysis is the best option because it can completely decolourize dye wastewater quicker than many other wastewater treatment methods. It is not only capable of treating wastewater, but because of its regeneration potential, it is also capable of being a sustainable treatment technology for dye wastewater [7].

Titanium dioxide is one of the primary photocatalysts used in the degradation of dye wastewater [8-13]. While seeing an influx of research related to using this constituent, TiO₂ has been used as a semiconductor since inaugural research occurred in the 1960s at the University of Tokyo [14]. Titanium dioxide has many advantages–it is non-toxic, there are many methods of synthesis available to the researchers and it is versatile in photocatalysis applications [15,16]. Also, TiO₂ has been expressed as being the most useful in environmental applications [17]. However, throughout literature it has been discovered that one of the biggest issues with using titanium dioxide is the band gap energy, an estimated 3.2 eV [18-21].

This eliminates the opportunity for TiO_2 to be used with light sources less than the measured band gap energy of 385 nm. As a result, TiO_2 nanocatalysts are insufficient in being used in visible light [22]. Therefore, research has been conducted by combining TiO_2 with a transition metal in a process known as doping.

There are three advantages of using transition metals to augment TiO_2. First, transition metals increase a photoreaction by increasing the surface area. Second, doped TiO_2 nanocatalysts trap electrons within band gaps forming anions. Anion formation increases dye decolourization [23]. Third, the augmentation of TiO_2 with transition metals develops a sustainable treatment method making this a more cost effective treatment process. Instead of the high costs and safety hazards associated with using UV lamps, photo-oxidation can be performed under various light sources, such as simulated or actual solar light [24-26]. Finally, doped-TiO_2 also has the potential of being reused following purification [27,28].

The transition metal used for doping in this work is cobalt (Co^{3+}). Cobalt is a transition metal with high reduction potential; its Co^{3+} ions trap conduction electrons. As a result, Co^{3+} ions are oxidized to Co^{2+}. Cobalt ions can also initiate p-type conductivity at the surface of the TiO_2. This provides an easier pathway for holes to move from the valence band to the surface of the catalyst [29] enhancing the photocatalytic activity. When a Co-doped TiO_2 catalyst is excited, it will react with superoxide anions. This ultimately prevents the potential of electron-hole recombination. The prevention of recombination maintains high photocatalytic productivity [30].

The aim of this paper is to explore the effects of pollutant and catalyst concentrations on wastewater decolourization while using cobalt-doped titanium dioxide (Co-doped TiO_2). Research on wastewater treatment by Co-doped titanium dioxide has been well documented [21,31-37]. Yet, while the degradation of a pollutant using Co-doped TiO_2 is evident, these texts have been limited to only discussing the effects of varying the TiO_2:Co ratio on photocatalytic degradation. There is little attention paid towards the effects of varying both the pollutant and photocatalyst concentrations. Therefore, this work will focus on varying both the concentration of wastewater and the photocatalyst loading on the decolourization of photocatalysis by Co-doped titanium dioxide nanocatalysts at a constant molar ratio.

EXPERIMENTAL

Doped TiO_2 sample preparation: Co-doped TiO_2 photocatalysts were synthesized using a conventional solid-state reaction method. Butler *et al.* [38] describes the process. In this study however, anatase TiO_2 and Co powders (> 99 %) were used.

Characterization of doped-TiO_2 photocatalysts: The crystalline phase of Co-doped TiO_2 was identified by an X-ray powder diffractometer (XRD) with CuK_α radiation ($\lambda = 0.15406$ nm) (Rigaku D/Max-II). An X-ray photoelectron spectroscopy (XPS; VGS Thermo K-Alpha, Waltham, MA) with AlK_α radiation identified the surface chemical composition of the Co-doped TiO_2 where the binding energies are referenced to the C 1s peak at 284.3 eV. The UV-visible spectra were determined using a

UV-visible recording spectrophotomer (V-600, Jasco) with an integrated sphere. Nitrogen adsorption approach (Micromeritics ASAP 2000, Norcross, GA) determined the Brunauer-Emmett-Teller (BET) specific surface areas and pore size distribution of Co-doped TiO_2.

Photocatalysis of acid orange 7: The catalytic vessel used in the degrading of acid orange 7 (AO7) was a 250 mL Pyrex glass vessel on a magnetic stirrer. This study focused on acid orange 7 due to it being commonly found in both the food and textile industries. In this study, three initial concentrations of acid orange 7 (24, 34 and 44 mg/L) were prepared with a volume of 100 mL. Irriadiation was accomplished using a UVB lamp with emission in the 200-800 nm range. At each concentration, Co-doped TiO_2 three photocatalyst loadings were prepared 0.025, 0.05 and 0.10 g in the 100 mL acid orange 7 aqueous solution. A control was prepared at all three concentrations. These samples had no photocatalyst present. Before UVB illumination, the dye wastewater and photocatalyst solution was magnetically stirred in the dark to reach adsorption-desorption equilibrium. The reaction times were set at 30, 60, 119 and 180 min. At each reaction time, the supernatant was collected and analyzed by a UV-visible spectrometer (Spectronic Genesys 20). Recorded absorbance values for samples were completed at a wavelength of 484 nm, the maximum absorbent wavelength of acid orange 7 dye. Samples were analyzed for the effectiveness of the TiO_2-based photocatalysts to decolourize acid orange 7 dye. The calculation of acid orange 7 dye efficiency of decolourization was determined by using the following equation:

$$\text{Decolourization } (\%) = \left(\frac{(AO7)_i - (AO7)_f}{(AO7)_i} \right) \times 100 \quad (1)$$

where $(AO7)_i$ is the initial acid orange 7 concentration (mg/L); $(AO7)_f$ is the final acid orange 7 concentration (mg/L).

RESULTS AND DISCUSSION

Characterization of Co-doped TiO_2: The XRD patterns of Co-doped TiO_2 powders calcinaed at 600 °C for 4 h in air are shown in Fig. 1. The pattern shows that the prepared Co-doped TiO_2 has diffraction patterns similar to JCPDs71-1166. This confirmed the successful preparation of anatase-phase TiO_2 with a minor rutile phase as listed in JCPDs 78-1508. In addition, Co^{3+} ions are inserted into the crystal lattice of TiO_2 and substituted for Ti^{4+} ions to form Co-O-Ti structures. This occurs because the ion radius of Co^{3+} (0.55 Å) is close to Ti^{4+} (0.68 Å) [39]. Based on the XRD results, we determined that even a tiny amount of doped Co^{3+} can transition TiO_2 from anatase to the rutile phase. Lattice parameters and unit cell volumes were calculated from the corresponding XRD patterns and are listed in Table-1.

The scanning electron microscopy (SEM) images and the energy dispersive spectroscopy (EDS) analysis results of Co-

TABLE-1 LATTICE PARAMETERS AND CELL VOLUMES OF 2 MOLE % CO-DOPED TiO_2 POWDERS			
	a	b	c
Co-doped	3.7793	3.7793	9.4918	135.6
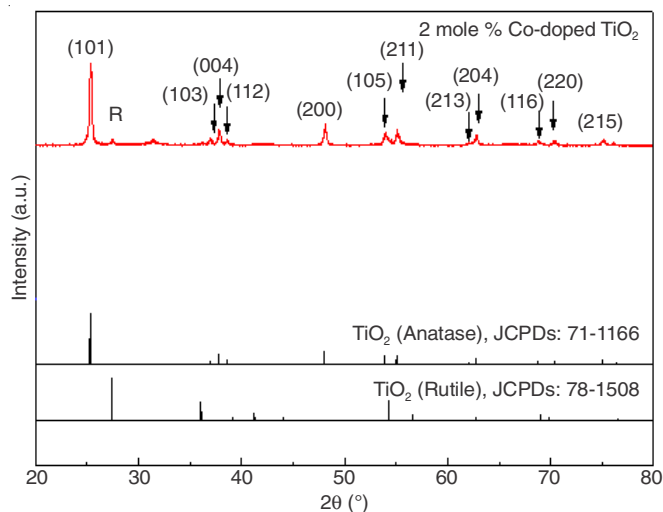
Fig. 1.   XRD pattern of 2 mole % Co-doped TiO$_2$ prepared by solid state reaction technique

doped TiO$_2$ powders are provided in Fig. 2. It was revealed that the grain sizes of Co-doped TiO$_2$ were uniformly distributed in the range of 100-200 nm. The grains formed significant agglomeration. The results from the EDS indicate that the Co element composition of the Co-doped TiO$_2$ nanocatalyst is slightly higher than the expected stoichiometric composition.

The elemental compositions and chemical status of the surface of Co-doped TiO$_2$ powder was further analyzed by XPS. The full range survey of XPS spectra of 2 mol % Co-doped TiO$_2$ powder is shown in Fig. 3(a). The main peaks are C 1s, Ti 2p, O 1s and Co 2p, centered at 284.9, 458.6, 530.0

Element	Weight (%)	Atomic (%)
O K	56.16	79.42
Ti K	42.60	20.11
Co K	1.22	0.47
Totals	100.00	
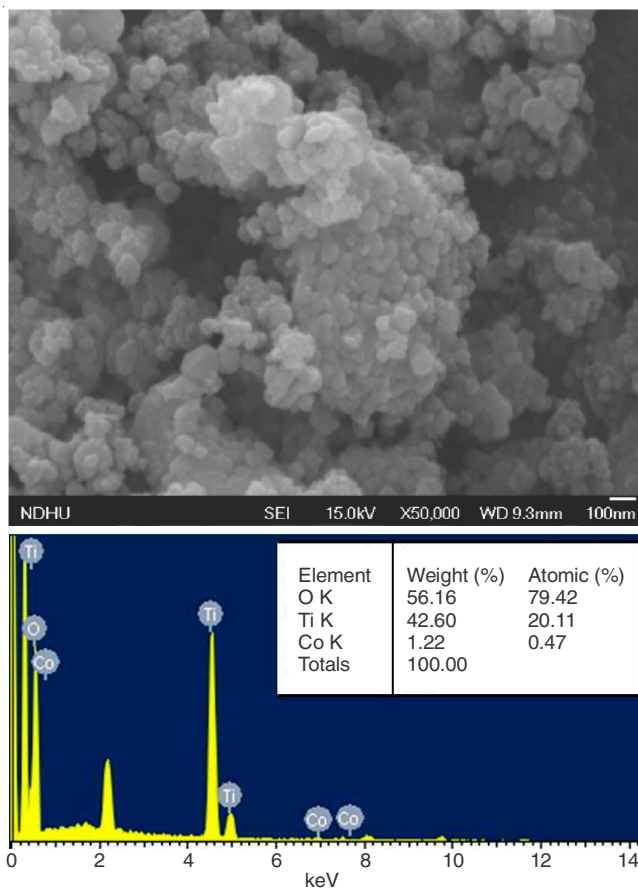
Fig. 2.   SEM images and EDS results of 2 mole % Co-doped TiO$_2$ spectra of the 2 mole % Co-doped TiO$_2$
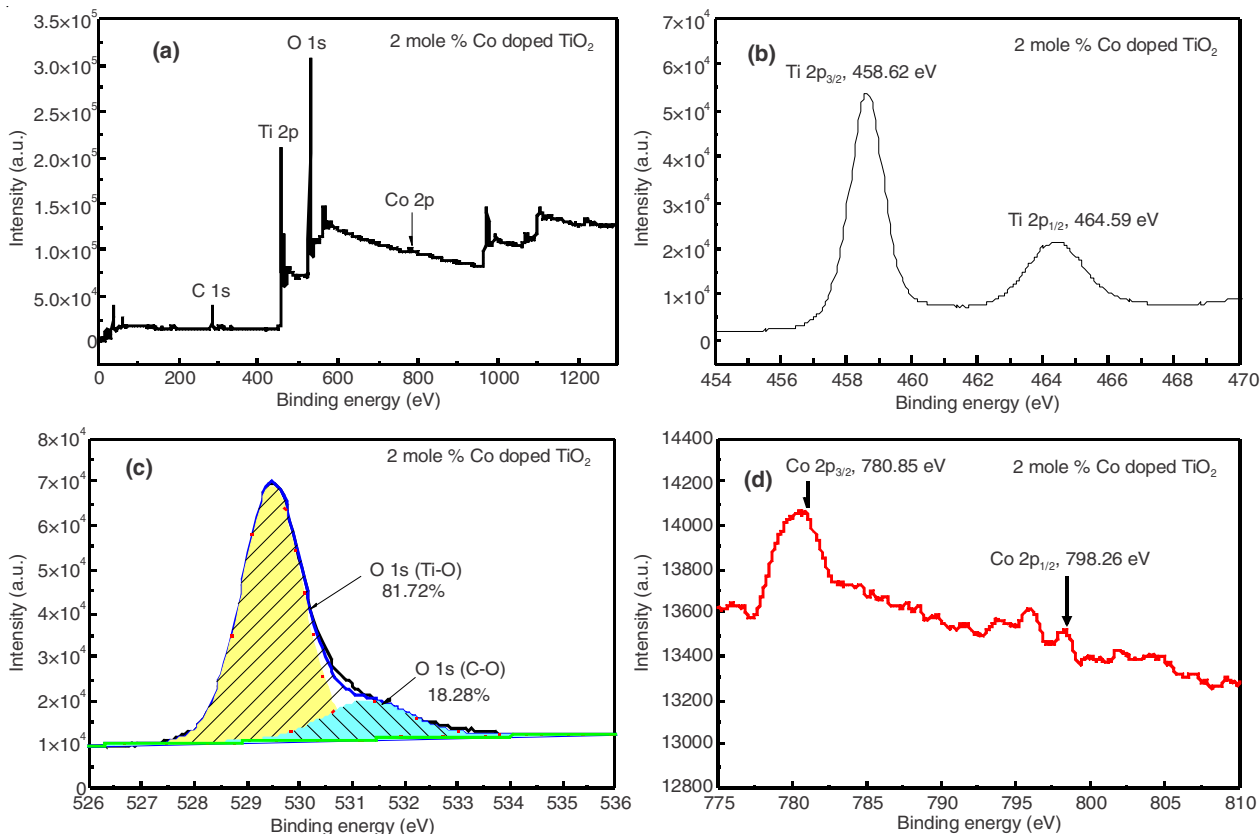
Fig. 3.   XPS spectra of the 2 mole % Co-doped TiO$_2$: (a) wide-survey spectrum; (b) Ti 2p core level spectrum; (c) O 1s core level spectrum; (d) Co 2p spectrum

and 780.1 eV, respectively. The carbon peak for C 1s located at 284.9 eV. This is due to the formation of adventitious carbon at the surface. Ti 2p core level spectrum obtained from the Co-doped TiO_2 powder is shown in Fig. 3(b). As shown from the figure, the Ti $2p_{1/2}$ and Ti $2p_{3/2}$ spin-orbital splitting photoelectrons were found at 464.6 and 458.6 eV, respectively.

These results correspond to results found in literature for the presence of Ti^{4+} [40]. The XPS photopeak of O 1s was fitted by multiple Gaussians as shown in Fig. 3(c). The O 1s spectrum was asymmetric and the main peak of O 1s was found at 529.5 eV. This is because of the oxygen molecules in TiO_2. There were two peaks observed at binding energies of 529.5 and 531.2 eV. These were attributed to the Ti-O and C-O groups with corresponding ratios of 81.7 and 18.3 % [41,42]. The XPS signals of Co 2p were weak in Co-doped TiO_2 as shown in Fig. 3(d). This was likely caused by low doping levels. The binding energies of 2p3/2 and 2p1/2 Co^{3+} were approximately 780.9 and 798.3 eV. These binding energies are very close to those in Co_2O_3 (780.9 eV for 2p3/2) [43]. Overall, Co is in a trivalent form within the Co-doped TiO_2 powder.

The N_2 adsorption-desorption isotherms and pore diameter distributions of Co-doped TiO_2 were further analyzed using N_2 adsorption. As presented in Fig. 4(a), Fe-doped TiO_2 adsorption-desorption isotherms are type IV with porous structures exhibiting a H3-type hysteresis loop. According to Langmuir classification, the results from this test indicated with the characteristics of mesoporous materials [44]. The adsorption isotherm exhibits a sharp inflection at a relative pressure between 0.80 and 0.90, suggesting the presence of a well-defined mesoporosity in the samples. The BET surface area for Co-doped powder was 24.1 m^2/g as shown in Table-2. The pore size distribution curves of for Co-doped TiO_2 is shown in Fig. 4(b). The average pore diameter of Fe-doped TiO_2 is 3.6 nm. There were two peaks to be found, one peak at 3.9 nm, while the second at 17.9 nm.
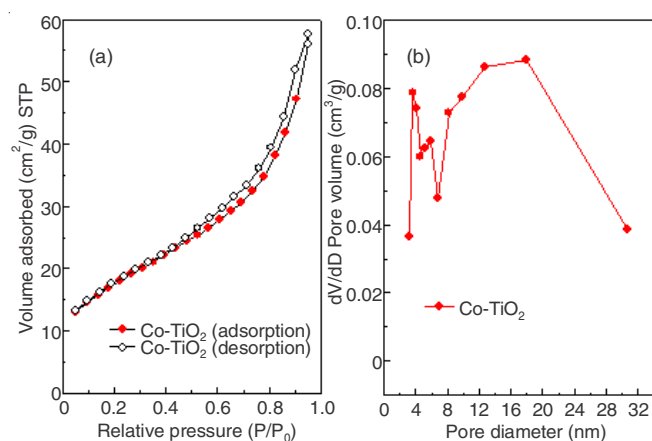
Fig. 4. (a) Nitrogen adsorption-desorption isotherms and (b) BJH pore size distributions of 2 mole % Co-doped TiO_2 powder

TABLE-2
BET SURFACE AREA, BJH SURFACE AREA AND PORE SIZE OF 2 MOLE % CO-DOPED TiO_2 POWDER PREPARED BY SOLID-STATE REACTION CALCINED AT 600 °C

Sample	BET surface area A (m^2/g)	BJH surface area A (m^2/g)	Pore volume V (cm^3/g)	Pore size (nm)
Co-doped	24.2	33.5	0.072	3.6

UV-visible absorption spectra of Co-doped TiO_2 powders were presented in Fig. 5. The absorption wavelengths (413.3 nm) appeared with band gaps at 2.93 eV.
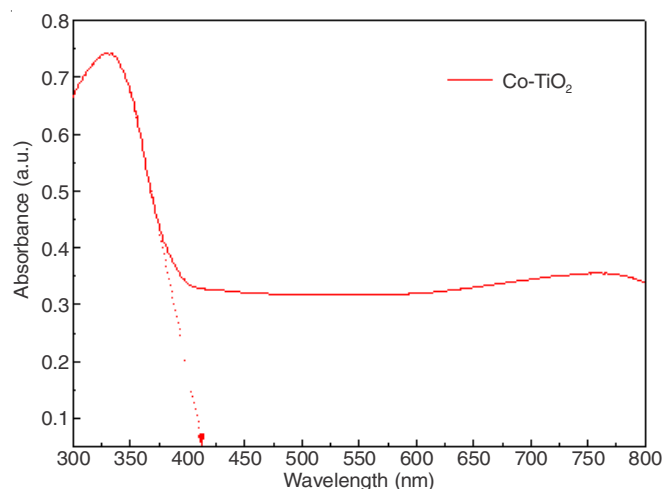
Fig. 5. UV-visible absorption spectra of 2 mole % Co-doped powder prepared by solid state reaction technique

Decolourization of acid orange 7

Effects of dye wastewater concentration: Results from the decolourization of acid orange 7 have been presented in Fig. 6(a-c). It was first discovered that the efficiency of decolourizing acid orange 7 by Co-doped TiO_2 is related to the initial dye concentration. In other words, as the initial concentration increases, the degradation of acid orange 7 decreases. Summarizing the results, at an initial concentration of 24 mg/L, the percent of dye decolourization observed was between 62.8 and 76.0 %. The range of decolourization decreased to 40.4-60.7 % at 34 mg/L. Finally, treatment dropped to 35.7-40.1 % when the initial concentration was 44 mg/L. This relationship has been confirmed in previous work by other authors degrading other pollutants [30,34,45,46].

There are two possible reasons for this trend. First, as the dye concentration increases, there is an increase in the equilibrium adsorption of dye on the surface of the catalyst. The increase of dye adsorption reduces the adsorption of $OH^•$, thereby decreasing the formation of hydroxyl radicals, an important component in decolourizing the dye. Second, because the dye concentration has increased, photons could have been adsorbed at the dye surface and not on the catalyst thereby decreasing the efficiency of photocatalysis [11,12,45,46].

Effects of photocatalyst loading: When the photocatalyst loading increases the treatment efficiency decreases [12,30]. In the experiment, this held true at 24 mg/L (Co-TiO_2 = 0.025 g, 76.0 %; Co-TiO_2 = 0.05 g, 64.4 %; Co-TiO_2 = 0.1 g, 62.8 %). However, as the dye concentration increased, the maximum treatment efficiency peaked when the photocatalyst loading was 0.05 g and then decreased at 0.1 g.

In principle, the increase of photocatalyst increases the overall number of active binding sites available thereby potentially producing more hydroxyl radical and superoxide anions. However, as the catalyst loading increases, binding sites can decrease. This is because the catalyst agglomerates and remains in suspension within the Pyrex glass vessel. As a
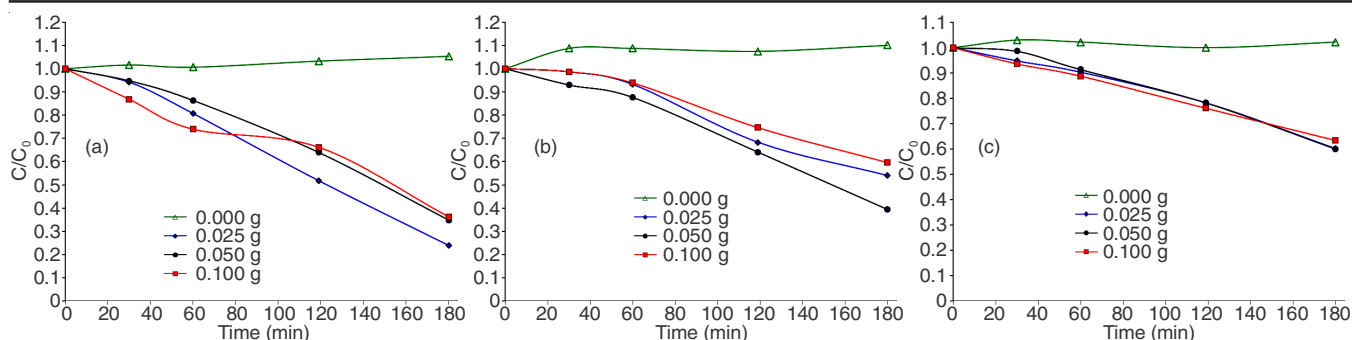
Fig. 6. Influences of doses of (a) Co-doped TiO$_2$ with an initial concentration of 24 mg/L, (b) Co-doped TiO$_2$ with an initial concentration of 34 mg/L and (c) Co-doped TiO$_2$ with an initial concentration of 44 mg/L, as monitored by changes in the absorbance at 484 nm: (a) Control; (b) 0.025 g; (c) 0.050 g; (d) 0.100 g
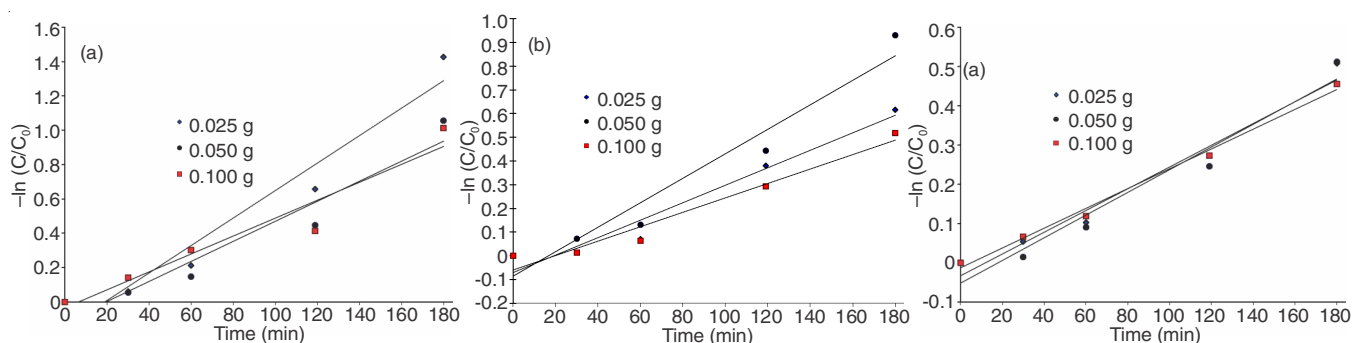
Fig. 7. Logarithmic plot the acid orange 7 dye colour removal using (a) Co-doped TiO$_2$ with an initial concentration of 24 mg/L, (b) Co-doped TiO$_2$ with an initial concentration of 34 mg/L and (c) Co-doped TiO$_2$ with an initial concentration of 44 mg/L, as monitored by changes in the absorbance at 484 nm: (a) Control; (b) 0.025 g; (c) 0.050 g; (d) 0.100 g

result, light cannot penetrate through the suspended catalyst ultimately decreasing photocatalyst activity [11,30,46]. In addition, the length of the photon path is shortened and allows for dye molecule to absorb the photons in contrast to the catalyst [47]. This was certainly evident when the dye concentration increased to 34 and 44 mg/L. A photocatalyst loading of 0.1 g was too high for high concentration of dye wastewater as Co-doped TiO$_2$ was limited its ability to degrade acid orange 7.

Kinetics of acid orange 7 photocatalytic degradation: Following treatment efficiency, it was necessary to determine the kinetic values for Co-doped TiO$_2$. Based on previous studies [48-50], photocatalytic degradation kinetics of dye wastewater followed first-order kinetics. In this study, we assumed that in all experiments, kinetics obeyed the first-order reaction model. Therefore, experimental rate constants (k$_{exp}$) were determined based on the first-order kinetics:

$$\ln\left(\frac{C_0}{C_t}\right) = k_{exp}t \qquad (2)$$

where C$_0$ is the initial concentration (mg/L), C$_t$ is the concentration at time t (mg/L) and k$_{exp}$ is the rate constant (time^{-1}).

If we assume that dC/dt = k$_{exp}$C$_0$ and the integration is ln(C$_0$/Ct) = k$_{exp}$t, the plot of ln(C$_0$/C$_t$) *versus* irradiation time (t) is a straight line and the slope is the rate constant k$_{exp}$. Fig. 7(a-c) are plots of –ln(C$_t$/C$_0$) *versus* treatment time of Co-doped TiO$_2$ with different photocatalyst loadings in the range of 0.025 g to 0.1 g/100 mL acid orange 7 and three different dye concentrations (24, 34 and 44 mg/L). These results can be found in Fig. 7a-c.

In summary, all the three graphs of -ln(C$_t$/C$_0$) *vs.* time yield a good linear relationship for photocatalytic degradation of acid orange 7 using Co-doped TiO$_2$ as photocatalyst. The kinetics of photocatalytic degradation by Fe-doped TiO$_2$ obey the first-order kinetic rate. Asiltürk *et al.* [47] observed similar trends with the degradation of malachite green dye using Fe-doped TiO$_2$. The calculated results for experimental rate constants, (k$_{exp}$) and R squares are listed in Table-3.

TABLE-3
EXPERIMENTAL RATE CONSTANT (k$_{exp}$) AND R SQUARE VALUES FOR CO-DOPED TiO$_2$ WITH VARIOUS DOSES (0.025, 0.050 AND 0.100 g) AND VARIOUS CONCENTRATIONS (24, 34 AND 44 mg/L)

Sample	k$_{exp}$ (min^{-1})	R^2
24 mg/L		
0.025 g	0.0080	0.945
0.050 g	0.0057	0.930
0.100 g	0.0051	0.927
34 mg/L		
0.025 g	0.0037	0.956
0.050 g	0.0052	0.948
0.100 g	0.0030	0.958
44 mg/L		
0.025 g	0.0028	0.961
0.050 g	0.0029	0.955
0.100 g	0.0025	0.993

In addition, having analyzed the corresponding data for each photocatalyst loading, as the dye wastewater concentration increases, the (k$_{exp}$) value peaks at a photocatalyst loading

of 0.05 g with the exception of when the dye concentration was 24 mg/L. These results correspond with trends found when reviewing the decolourization of acid orange 7.

Conclusion

The effects of varying wastewater strength and photocatalyst loading on the photocatalytic degradation of acid orange 7 by Co-doped TiO_2 photocatalyst under UV irradiation have been studied. From the results, it was determined that as the dye wastewater concentration increased the photocatalytic degradation decreased. As the dye concentration increased, the most efficient photocatalytic loading observed was 0.05 g. Higher doses of photocatalyst were observed to be ineffective as the particles remained suspended within the vessel preventing light from penetrating through. These are important findings because they indicate that there exists a plateauing point at which the nanocatalyst concentrations swing from having positive removal effects, to hindering the removal process. This could help in reducing the cost of materials and the time and effort necessary to synthesize the catalysts and perform the treatment. This relationship is explained using first-order kinetics, which is consistent with previous studies of Co-doped TiO_2 dye wastewater decolourization.

REFERENCES

1. J. Zhang, Y. Zhang, X. Quan, Y. Li, S. Chen, H. Zhao and D. Wang, *Biochem. Eng. J.*, **63**, 31 (2012).
2. Y. Li and D. Xi, *Environ. Sci. Poll. Res.*, **11**, 372 (2004).
3. B. Smith, G. O'Neal, H. Boyter and J. Pisczek, *J. Chem. Technol. Biotechnol.*, **82**, 16 (2007).
4. X. Lu, L. Ma, Z. Wang and M. Huang, *J. Environ. Eng. Sci.*, **27**, 493 (2010).
5. X. Zhao and I.R. Hardin, *Dyes Pigments*, **73**, 322 (2007).
6. US Environmental Protection Agency, Ozone for Industrial Water and Wastewater Treatment: A Literature Survey, EPA-600-2-80-060 (1980).
7. H. Kusic, N. Koprivanac and A.L. Bozic, *J. Photochem. Photobiol. Chem.*, **252**, 131 (2013).
8. C. Hachem, F. Bocquillon, O. Zahraa and M. Bouchy, *Dyes Pigments*, **49**, 117 (2001).
9. A. Aguedach, S. Brosillon, J. Morvan and E.K. Lhadi, *Appl. Catal. B*, **57**, 55 (2005).
10. E. Bizani, K. Fytianos, I. Poulios and V. Tsiridis, *J. Hazard. Mater.*, **136**, 85 (2006).
11. U.G. Akpan and B.H. Hameed, *J. Hazard. Mater.*, **170**, 520 (2009).
12. M.A. Rauf, M.A. Meetani and S. Hisaindee, *Desalination*, **276**, 13 (2011).
13. M.N. Chong, Y.J. Cho, P.E. Poh and B. Jin, *J. Clean. Prod.*, **89**, 196 (2015).
14. A. Fujishima, T.N. Rao and D.A. Tryk, *J. Photochem. Photobiol. Chem.*, **1**, 1 (2000).
15. C. Hsieh, M. Lai and C. Pan, *J. Chem. Technol. Biotechnol.*, **85**, 1168 (2010).
16. A.A. Ismail and D.W. Bahnemann, *J. Mater. Chem.*, **21**, 11686 (2011).
17. J. Xu, L. Li, C. Guo, Y. Zhang and S. Wang, *Chem. Eng. J.*, **221**, 230 (2013).
18. J. Zhou, Y. Zhang, X. Zhao and A. Ray, *Ind. Eng. Chem. Res.*, **45**, 3503 (2006).
19. M. Zhou, J. Yu and B. Cheng, *J. Hazard. Mater.*, **137**, 1838 (2006).
20. R. Ullah, H. Sun, H.M. Ang, M.O. Tade and S. Wang, *Catal. Today*, **192**, 203 (2012).
21. M. Subramanian, S. Vijayalakshmi, S. Venkataraj and R. Jayavel, *Thin Solid Films*, **516**, 3776 (2008).
22. M. Stylidi, D. Kondarides and X. Verykios, *Appl. Catal. B*, **47**, 189 (2004).
23. I. Tatlidil, E. Bacaksiz, C.K. Buruk, C. Breen and M. Sokmen, *J. Alloys Comp.*, **517**, 80 (2012).
24. S. Ong, O. Min, L. Ho and Y. Wong, *Water Air Soil Pollut.*, **223**, 5483 (2012).
25. Y. Lv, L. Yu, X. Zhang, J. Yao, R. Zou and Z. Dai, *Appl. Surf. Sci.*, **257**, 5715 (2011).
26. J. Wang, J. Li, L. Zhang, C. Li, Y. Xie, B. Liu, R. Xu and X. Zhang, *Catal. Lett.*, **130**, 551 (2009).
27. N. Bao, Y. Li, X. Yu, J. Niu, G. Wu and X. Xu, *Environ. Sci. Poll. Res.*, **20**, 897 (2013).
28. V.G. Gandhi, M.K. Mishra and P.A. Joshi, *J. Ind. Eng. Chem.*, **18**, 1902 (2012).
29. D.B. Hamal and K.J. Klabunde, *J. Phys. Chem. C*, **115**, 17359 (2011).
30. M.A. Barakat, H. Schaeffer, G. Hayes and S. Ismat-Shah, *Appl. Catal. B*, **57**, 23 (2005).
31. C. Shifu, L. Wei, Z. Sujuan and C. Yinghao, *J. Sol-Gel Sci. Technol.*, **54**, 258 (2010).
32. R. Amadelli, L. Samiolo, A. Maldotti, A. Molinari, M. Valigi and D. Gazzoli, *Int. J. Photoenergy*, **2008**, 1 (2008).
33. M. Hamadanian, A. Reisi-Vanani and A. Majedi, *J. Iran. Chem. Soc.*, **7(S2)**, S52 (2010).
34. E.B. Gracien, J. Shen, X. Sun, D. Liu, M. Li, S. Yao and J. Sun, *Thin Solid Films*, **515**, 5287 (2007).
35. M. Iwasaki, M. Hara, H. Kawada, H. Tada and S. Ito, *J. Colloid Interface Sci.*, **224**, 202 (2000).
36. K. Esquivel, M.G. García, F.J. Rodríguez, L.A. Ortiz-Frade and L.A. Godínez, *J. Appl. Electrochem.*, **43**, 433 (2013).
37. R. Rahimi, E.H. Fard, S. Saadati and M. Rabbani, *J. Sol-Gel Sci. Technol.*, **62**, 351 (2012).
38. E.B. Butler, C.-C. Chen, Y.-T. Hung, M.S. Al Ahmad and Y.-P. Fu, *Integr. Ferroelectr.*, **168**, 1 (2016).
39. R.T. Shannon, *Acta Crystallogr. A*, **32**, 751 (1976).
40. L. Deng, S. Wang, D. Liu, B. Zhu, W. Huang, S. Wu and S. Zhang, *Catal. Lett.*, **129**, 513 (2009).
41. Q. Luo, X. Li, X. Li, D. Wang, J. An and X. Li, *Catal. Commun.*, **26**, 239 (2012).
42. C.-C. Chen, E. Butler, M.A. Ahmad, Y.-T. Hung and Y.-P. Fu, *Mater. Res. Bull.*, **50**, 178 (2014).
43. C.D. Wagner, W.M. Riggs, L.E. Davis, J.F. Moulder and G.E. Muilenberg, Handbook of X-ray Photoelectron Spectroscopy, Perkin Elmer, Eden Prairie (1979).
44. M. Kruk and M. Jaroniec, *Chem. Mater.*, **13**, 3169 (2001).
45. H.Y. He and P. Chen, *Chem. Eng. Commun.*, **199**, 1543 (2012).
46. I.K. Konstantinou and T.A. Albanis, *Appl. Catal. B*, **49**, 1 (2004).
47. M. Asiltürk, F. Sayýlkan and E. Arpaç, *J. Photochem. Photobiol. Chem.*, **203**, 64 (2009).
48. L. Luo, A.T. Cooper and M. Fan, *J. Hazard. Mater.*, **161**, 175 (2009).
49. H.J. Kim, Y.G. Shul and H. Han, *Top. Catal.*, **35**, 287 (2005).
50. S. Qourzal, M. Tamimi, A. Assabbane and Y. Ait-Ichou, *J. Colloid Interface Sci.*, **286**, 621 (2005).